Experimental Mechanics (2010) 50:1013–1021
DOI 10.1007/s11340-009-9296-8

Vibration Analysis of Perforated Plates Using Time-Average Digital Speckle Pattern Interferometry

G.G. Romero · E.E. Alanís · C.C. Martínez · L.G. Nallim · M.W. Toledo · L. Álvarez

Received: 28 March 2009 / Accepted: 12 September 2009 / Published online: 27 October 2009

Abstract Digital Speckle Interferometry is a non invasive full-field coherent optical technique used in mechanical vibration measurement. In this research, it is used for tuning resonant frequencies of vibrating plates in order to investigate the dynamical behavior of perforated plates. The plate was excited to resonant vibration by a sinusoidal acoustic source. Fringe pattern produced during the time-average recording of the vibrating plate, for several resonant frequencies were registered. Results of plates fixed at one edge having internal holes and attached masses are presented. Experimental natural frequencies and modal shapes are compared to those obtained by an analytical approximate solution based on the Rayleigh–Ritz method with the use of orthogonal polynomials as coordinate function. A high degree of correlation between computational analysis and experimental results was observed, proving the potentiality of the optical technique as experimental validation of the numerical simulations.

G.G. Romero (✉) · E.E. Alanís
Facultad de Ciencias Exactas - Grupo de Óptica Láser,
CIUNSa - Universidad Nacional de Salta,
Av. Bolivia 5150,
4400 Salta, Argentina
e-mail: marigra@unsa.edu.ar
e-mail: romeropelayog@gmail.com

C.C. Martínez
Facultad de Ciencias Naturales - Grupo de Óptica Láser,
CIUNSa - Universidad Nacional de Salta,
Av. Bolivia 5150,
4400 Salta, Argentina

L.G. Nallim · M.W. Toledo · L. Álvarez
Facultad de Ingeniería, Universidad Nacional de Salta,
Av. Bolivia 5150,
4400 Salta, Argentina

Keywords Digital speckle pattern interferometry · Vibration · Dynamic deformations · Computational analysis

Introduction

Plates having internal holes and attached masses are very important in many engineering applications [1–3]. Particularly, internal holes are necessary in plates due to operational conditions, namely passage of conduits or ducts, electrical conductors, etc. For these reasons this type of plates constitutes common structural elements used in naval as well as in ocean engineering. The accurate and efficient determination of the natural vibration frequencies and modal shapes of these components are essential to the design and performance evaluation of a mechanical system [4]. The inclusion of a free hole and concentrated masses in the vibrating plate formulation is the source of analytical difficulties and complex mathematical structures for the boundary conditions, making the exact analysis complicated even for the simplest cases. Consequently, most studies on these structural elements use approximate analytical or numerical methods. In many cases, experimental and computational methods can be combined so that the data obtained by one of the methods can be used by the other one to verify the results [5]. In this work, the system was studied analytically and experimentally. The determination of the natural frequencies and modal shapes of free transverse vibration of the vibrating plates was carried out by using an extension of a methodology presented in a previous work [6]. The developed analytical approach is based on the Rayleigh–Ritz method with the use of orthogonal polynomials as coordinate functions [7].

Although these types of plates are well suitable for dynamical analysis with approximated numerical method-

ologies, improvements and adjustments for both calculus possibilities and new material requirements are necessary. In this way, experimental verification as a supporting tool can provide measurements for eventual numerical methods adjustment. Accelerometers are commonly used for measuring frequency and amplitude of vibrations at certain point, but the main disadvantage of using an accelerometer is that it has to be in contact with the plate—adding weight to it—and sometimes, there is a noticeable change in stiffness of the plate component. Some optical techniques have been developed to give precise measurements of these mechanical parameters in a non invasive way. One of these, based on the theory of speckle decorrelation, was used for amplitude and frequency measurement of normal vibrations [8]. In a more recent paper [9] time resolved digital speckle pattern interferometry is used as an independent point sensor to measure time-resolved mechanical vibrations. The temporal resolution of these methods allows recording time histories for dynamic phenomena other than steady-state vibrations, and these data may be processed in the Fourier domain. Other optical interferometric techniques, like the one proposed in this paper [10–13] have an excellent spatial resolution but generally lack temporal resolution. Nevertheless, the high spatial resolution allows us to measure the full-field vibration amplitude by computing a fringe pattern.

One of the most exciting developments of speckle interferometry has been its ability to compare interferometrically wave fronts originated on a rough object surface in two different states of deformation [14, 15]. In Digital Speckle Pattern Interferometry (DSPI), a speckle pattern is formed by illuminating the surface of the object by a laser beam. The object wave is imaged on a CCD camera, where it is made to interfere with a reference wave. The resulting fringe map enables us to obtain a precise measurement of deformations undergone between the two object states. This technique is well suited to measure deformation in mechanical systems subjected to stress under several boundary conditions [16, 17]. Time-average DSPI is a non-contact-type full-field tool, appropriate to carry out measuring and monitoring of vibrations in the laboratory as well as in industries [18, 19]. In this work, real-time time-average DSPI was used for tuning natural frequencies of vibrating plates and for visualizing nodal lines and modal shapes. A comparison between computational analysis and experimental results shows a high degree of correlation.

Theoretical Aspects

Analytical Formulation

The general mechanical system shown in Fig. 1 is a vibrating rectangular perforated isotropic plate with edges

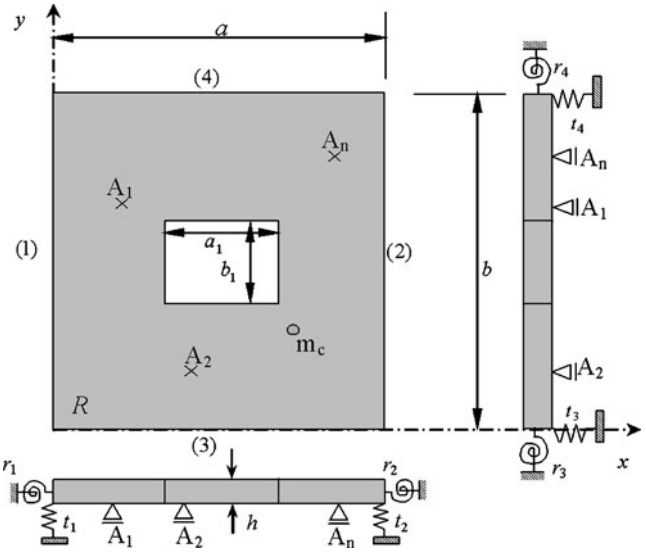

Fig. 1 General description of the perforated plate

elastically restraining against rotation and translation [20]. The plate has a concentrated mass rigidly attached to it and elastic point springs. The maximum kinetic energy of the plate freely vibrating with amplitude *W(x,y)* and radian frequency ω expressed in rectangular co-ordinates [21] is given by:

$$T_{\max} = \frac{\rho h \omega^2}{2} \iint_R W^2(x,y)\,dx\,dy + \frac{1}{2} m_c \omega^2 W^2(x_0, y_0), \qquad (1)$$

where ρ is the mass density of the plate material, h is the plate thickness, m_c is the concentrated mass placed in the point (x_0, y_0), and the integration is carried out over the entire plate domain R.

The maximum strain energy of the mechanical system is given by [6]:

$$U_{\max} = U_{p,\max} + U_{R,\max} + U_{T,\max} + U_{A,\max} \qquad (2)$$

$U_{p,\max}$ is the strain energy due to plate bending and is given by:

$$U_{p,\max} = \frac{1}{2} \iint_R D \left\{ \begin{array}{l} \left(\dfrac{\partial^2 W}{\partial x^2} + \dfrac{\partial^2 W}{\partial y^2} \right)^2 \\ -2(1-\mu) \left[\dfrac{\partial^2 W}{\partial x^2} \dfrac{\partial^2 W}{\partial y^2} - \left(\dfrac{\partial^2 W}{\partial x \partial y} \right)^2 \right] \end{array} \right\} dx dy \qquad (3)$$

where D is the flexural rigidity given by $D = Eh^3/[12(1-\mu^2)]$, in which E is the Young's modulo and μ is the Poisson's ratio. The maximum strain energy stored

in rotational and translational springs at the plate edges are:

$$U_{R,\max}=\frac{1}{2}\left[\begin{array}{l} r_1\int_0^b (W_x(0,y))^2dy + r_2\int_0^b (W_x(a,y))^2dy \\ + r_3\int_0^a \left(W_y(x,0)\right)^2dx + r_4\int_0^a \left(W_y(x,b)\right)^2dx \end{array}\right] \tag{4}$$

and

$$U_{T,\max}=\frac{1}{2}\left[\begin{array}{l} t_1\int_0^b (W(0,y))^2dy + t_2\int_0^b (W(a,y))^2dy \\ + t_3\int_0^a (W(x,0))^2dx + t_4\int_0^a (W(x,b))^2dx \end{array}\right] \tag{5}$$

respectively.

The constants r_i and t_i (i=1,...,4) are the rotational and translational spring parameters along the corresponding edges. Finally, the maximum strain energy stored in the N_p elastic point springs—which in the limiting case ($c_p\to\infty$) can represent pinned supports—is given by:

$$U_{A,\max}=\frac{1}{2}\sum_{i=1}^{N_p} c_{p,i}W^2(x_i,y_i) \tag{6}$$

where $c_{p,i}$ are the translational spring parameters of the elastic supports placed in the coordinates (x_i, y_i). Then, in the general case depicted in Fig. 1, the energy functional results in:

$$F[W]=T_{\max}-U_{\max} \tag{7}$$

The plate deflection is represented by two sets of beam characteristic orthogonal polynomials, $\{p_i(x)\}$ and $\{q_j(y)\}$, as

$$W(x,y)=\sum_i\sum_j c_{ij}p_i(x)q_j(y) \tag{8}$$

where c_{ij} are the unknown coefficients to be minimized in the Rayleigh–Ritz method.

The procedure for the construction of the orthogonal polynomials has been developed by Bhat [6, 22] and is applied in this paper following the same scheme outlined in reference [4] for perforated plates. Substituting the approximate function (8) into equation (7) and later application of the Ritz method leads to the following governing equation:

$$\sum_i\sum_j \left[K_{ijkh}-\omega^2M_{ijkh}\right]c_{ij}=0 \tag{9}$$

Equation (9) yields an eigenvalue determinant, whose zeros give the natural frequencies of the plate. Back substitution yields the coefficient vectors; substitution of these coefficient vectors into equation (7) gives the mode shapes of the plate.

Out-of-plane Dynamic Deformation Analysis

A schematic of DSPI setup to measure out-of-plane or transverse vibrations is shown in Fig. 2.

In a typical experiment, when the object is stationary in equilibrium, irradiance $I_0(x,y)$ produced by interference of the object and reference field is given by [14]:

$$I_0(x,y)=I_{ob}(x,y)+I_{re}(x,y) + 2[I_{ob}(x,y)I_{re}(x,y)]^{1/2}\cos[\varphi(x,y)] \tag{10}$$

where $I_{ob}(x,y)$ and $I_{re}(x,y)$ are the intensities at the co-ordinate (x,y) of the object and reference beam respectively, and $\varphi(x,y)$ is the phase difference between the two interfering beams, which is assumed to be randomly distributed.

Once the stationary irradiance I_0 is registered, the plate is excited to resonant frequencies by a sinusoidal acoustic source which provides a continuous range of audio frequencies. In Fig. 2, if normal illumination and viewing directions are assumed, $\boldsymbol{K}_1=-\boldsymbol{K}_2$ and if the CCD camera frame integration time is much longer than the vibration period of the plate in a single exposure during which the object is vibrating harmonically, the time-average intensity is given by:

$$I_{av}(x,y)=I_{ob}(x,y)+I_{re}(x,y) + 2[I_{ob}(x,y)I_{re}(x,y)]^{1/2}\cos[\varphi(x,y)]J_0[k(x,y)] \tag{11}$$

where, J_0 is a zero-order Bessel function and, assuming that the object is vibrating in one of its resonant modes, at a single frequency f, the argument $k(x,y)$ is given by:

$$k(x,y)=4\pi a(x,y)/\lambda \tag{12}$$

where $a(x,y)$ is the amplitude vibration at the point (x,y) of the plate. Subtracting from equation (11) the reference irradiance I_o given by equation (10), the resulting intensity is:

$$I(x,y)=2[I_{ob}(x,y)I_{re}(x,y)]^{1/2}\cos[\varphi(x,y)] \times(1-J_0[k(x,y)]) \tag{13}$$

That is, the speckle brightness is spatially modulated by the Bessel function J_0. The fringe pattern of equation (13) provides time-averaged information about the vibration

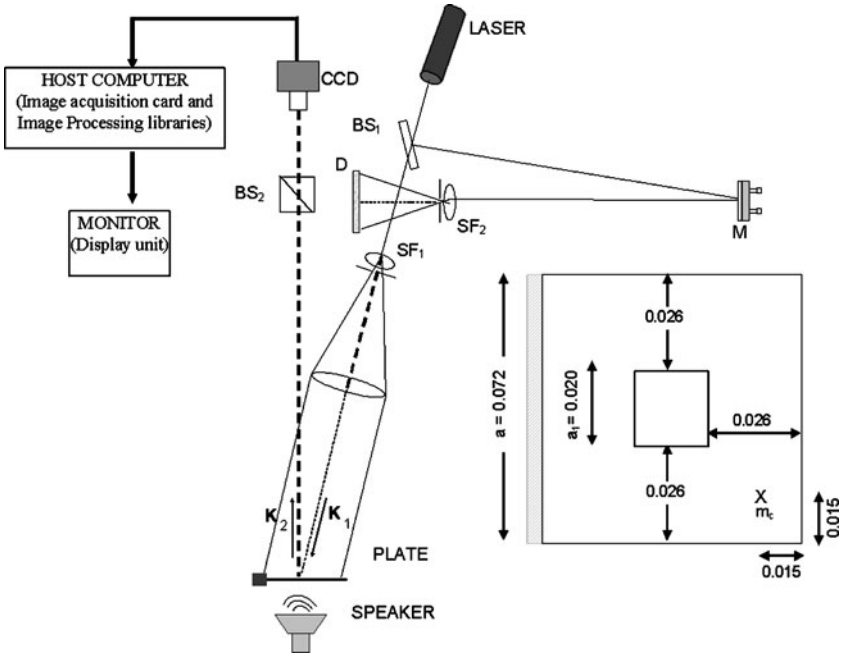

Fig. 2 Optical set-up. *BS* beam splitter; *SF* spatial filter; *M* mirror; *D* difuser; $\mathbf{K}_1$, incident vector; $\mathbf{K}_2$, scattering vector. The inset shows the plate and its linear dimensions in meters

amplitude in which the nodal regions are easily identified because their fringes are much darker than the other fringes, as it is explained in "Experiments and Results." A resonant condition of the object is easily achieved by looking at the fringes displayed on the monitor while tuning the audio generator until a stationary fringe pattern is observed.

Experiments and Results

As it is shown in Fig. 2, the DSPI set-up for recording the fringe pattern of dynamic deformation is basically a simple interferometer in which a laser beam (He-Ne, 632.8 nm) is split into two by a beam splitter, BS_1. One of these beams, previously expanded and collimated, illuminates the surface of the plate under study. After being redirected by the mirror M, the other beam, used as reference beam, is expanded and illuminates a diffuser D. At the beam splitter cube BS_2 both beams are combined to form a speckle interferogram which is imaged by a monochrome TV camera. The CCD sensor of the camera is an array of 768×572, 8.4 μm square pixels. The video analog output is digitized at 256 levels of gray and stored in a buffer of a MATROX PULSAR frame grabber. A Visual Basic 6.0 based program was developed to acquire process and display the speckle interferogram. In Fig. 2, vectors $\boldsymbol{K_1}$ and $\boldsymbol{K_2}$ define the illumination and observation directions, respectively.

The plate, which is made of aluminum, has a rectangular perforation in its center. In Table 1, geometrical, mechanical and dimensionless parameters used in computational simulations are listed.

After optical system alignment, an image of the plate at rest is grabbed by the CCD camera and stored in the frame grabber memory, constituting this image the reference state. By means of a speaker driven by an audio generator, energy is given to the plate, in which vibration is induced at continuously varied frequencies. The successive time average interferograms are subtracted from the reference one giving rise to a transient interference pattern that is displayed in real time on the computer screen until a resonant mode is tuned in, in which case, a stationary pattern can be seen. Once this condition is attained, the resonant frequency is measured from the signal generator, previously calibrated by means of an oscilloscope.

Modal Shapes and Nodal Patterns

The particular case verified by means of the experimental technique is generated from the general analytical approach

Table 1 Geometrical and mechanical parameter of the test object

Plate thickness	$h=0.98\times10^{-3}$ m
Poisson modulo	$\mu=0.35$
Young modulo	$E=6.82\times10^{10}$ N/m^2
Mass density	$\rho=2{,}86\times10^{3}$ Kg/m^3
Flexural stiffness	$D=6.1$ Nm
Plate length/height relation	a/b=1
Plate/perforation relation	$a_1/b=0.277$
Plate mass	$M=17.83\times10^{-3}$ Kg
Concentrated mass	$m_c=2.00\times10^{-3}$ Kg
Concentrate mass/plate mass relation	m/M=0.112171

presented in "Analytical Formulation," taking $r_1 \rightarrow \infty$, $t_1 \rightarrow \infty$ and $r_1 \rightarrow 0$, $t_i \rightarrow 0$ (i=1,2,3), so that a cantilever plate is obtained.

In Fig. 3(a), three interferograms corresponding to different resonant frequencies for the plate, clamped on its left edge, are shown. Several fringes of different speckle contrast can be seen, each one representing regions of constant vibration amplitude. The darkest fringes represent nodal regions. For the same resonant frequencies, the modal patterns and the nodal lines calculated by means of analytical methods are shown in Fig. 3(b) and (c) respectively. A remarkable agreement between the calculated modal shapes and the corresponding fringe patterns can be observed. Resonant frequencies are indicated in each diagram.

To investigate the effect of the concentrated mass on the natural frequencies and the corresponding modal shapes, a concentrated mass (m_c) was added to the plate near its right

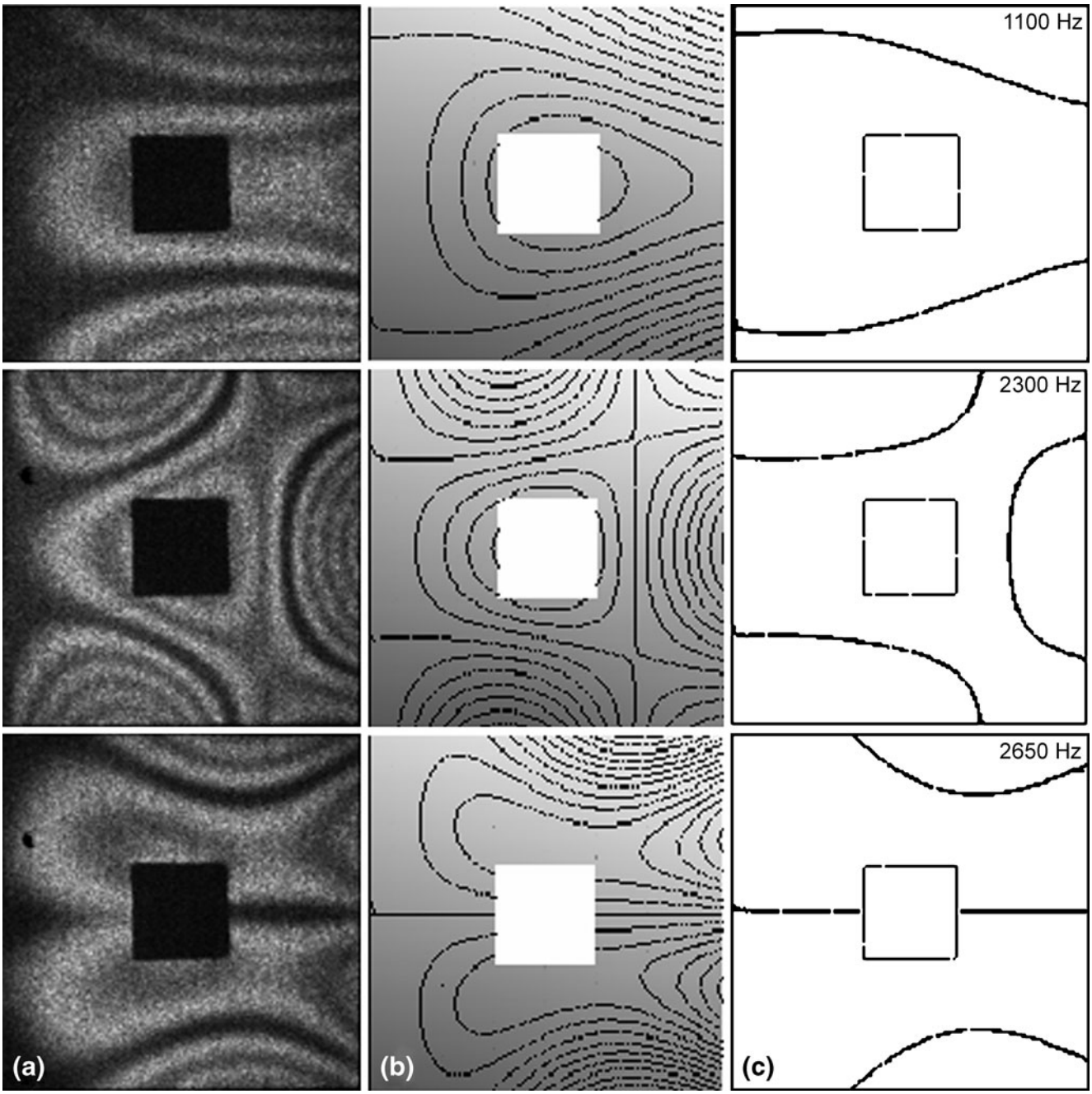

Fig. 3 Experimental and analytical results for the perforated plate, vibrating at different resonant frequencies: (**a**) interferogram, (**b**) calculated modal shapes and (**c**) calculated nodal pattern. The plate is clamped on the left edge

bottom corner, marked with a cross in Fig. 2. The results obtained both by the analytical and experimental methods are shown in Fig. 4, where asymmetries in the fringe patterns, with respect to the horizontal middle axis of the plate, are observed.

Resonant Frequencies Calculations

The analytical method distinguishes each resonant mode by means of a dimensionless frequency parameter ω in equation (9). The resonant frequencies, f, are related to this parameter by means of the expression,

$$\omega = \left(\sqrt{\frac{\rho h}{D}} 2\pi a^2\right) f \tag{14}$$

therefore,

$$f = \left(\frac{1}{2\pi a^2}\sqrt{\frac{D}{\rho h}}\right)\omega \tag{15}$$

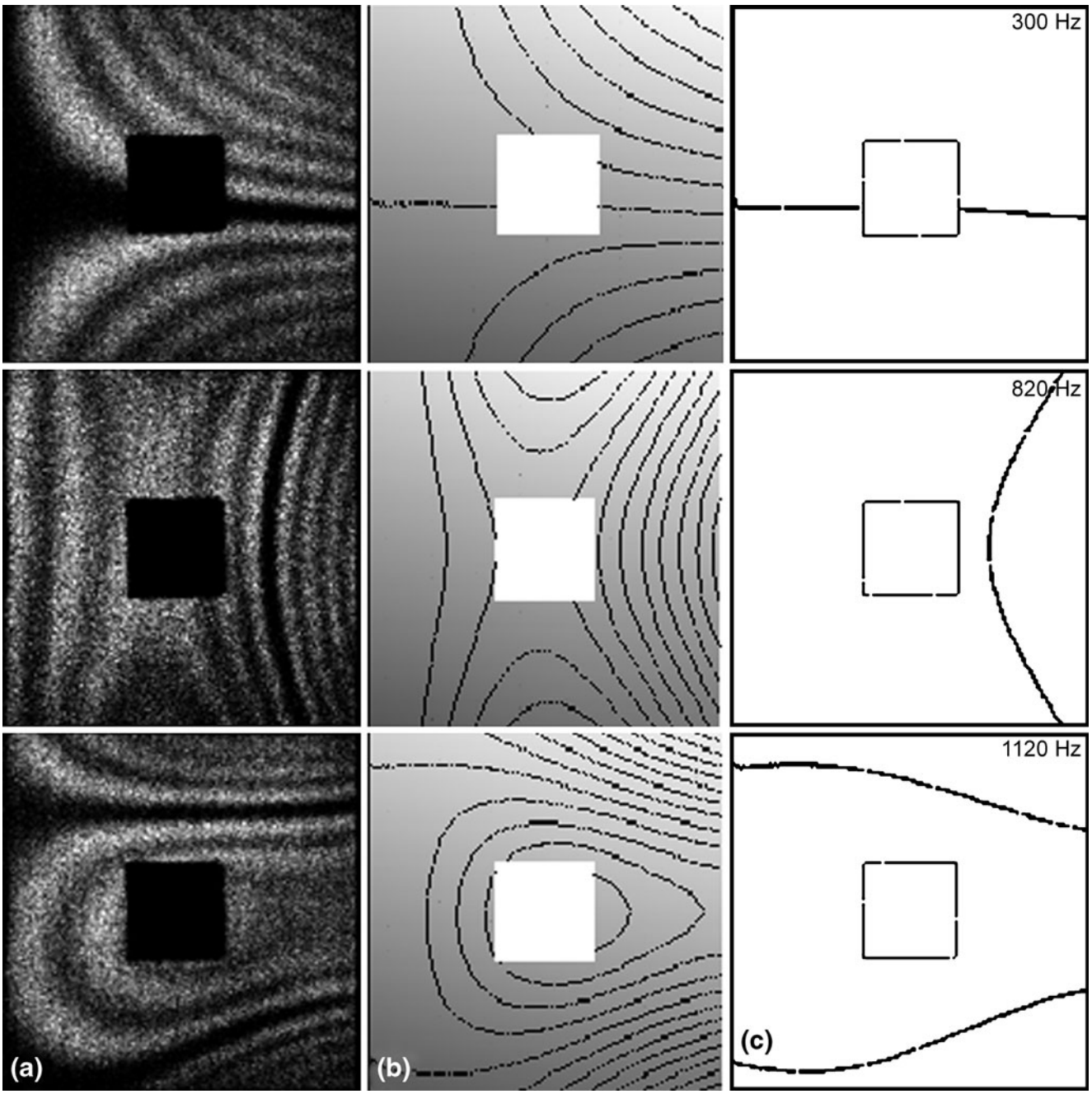

Fig. 4 Experimental and analytical results for the perforated plate, having a concentrated additional mass, vibrating at different resonant frequencies: (**a**) interferogram, (**b**) calculated modal shapes and (**c**) calculated nodal pattern. The plate is clamped on the left edge

The values of the frequencies measured experimentally and the corresponding values calculated by the analytical method and equation (15) are compared in Fig. 5, where plots of the experimental frequencies as a function of the analytical ones are shown. The frequencies of the plate with and without a concentrated mass are shown in Fig. 5(a) and (b), respectively. Linear regressions between calculated and measured frequencies are represented by a line in both figures showing a high degree of correlation as the correlation coefficient r^2 suggests. The main errors of the measured frequencies arise from the appreciation of the signal generator scale. These are estimated to be 1% approximately. The differences between experimental frequency values and the corresponding analytical ones are attributed to the measurement of the parameters involved in the coefficient $(\sqrt{\frac{\rho h}{D}}2\pi a^2)$ of equation (14), which error was estimated to be 2%.

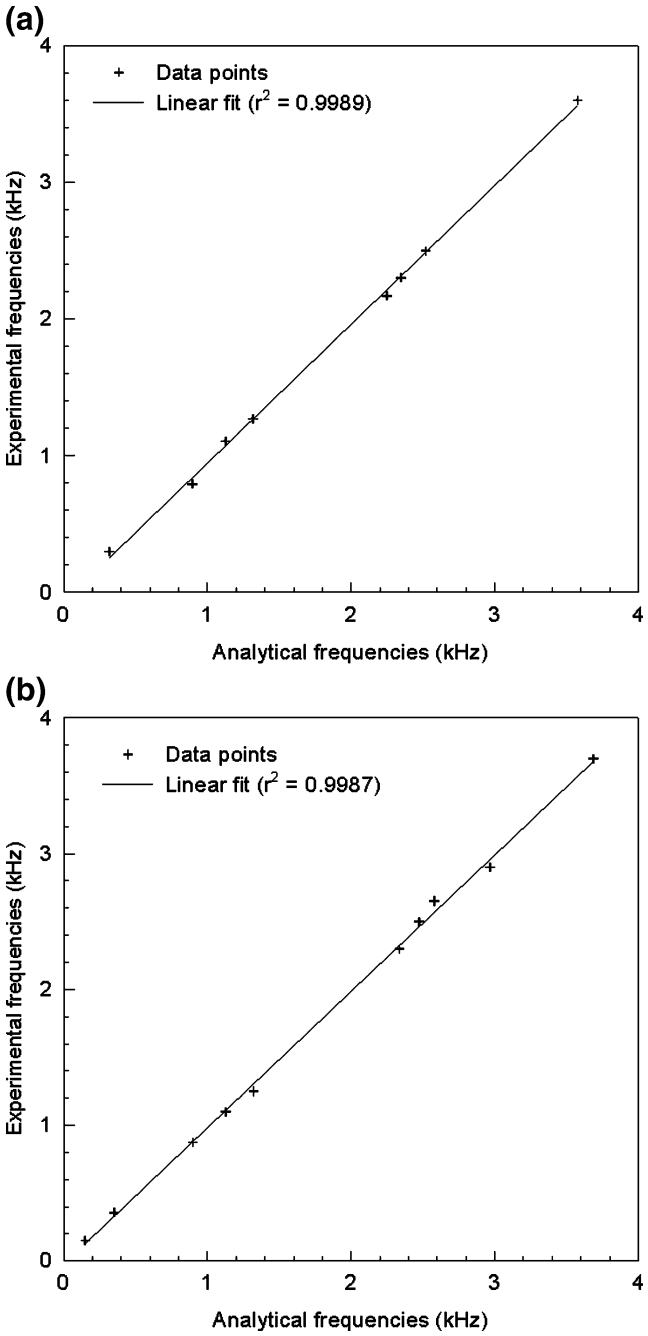

Fig. 5 Correlation between measured and calculated frequencies for a perforated plate clamped on one edge: (**a**) with a concentrated additional mass (**b**) without a concentrated additional mass

Amplitude Measurements

As indicated in "Out-of-plane Dynamic Deformation Analysis", from equation (12), the vibration amplitude can be calculated as:

$$a(x,y) = k(x,y)\lambda/4\pi \tag{16}$$

in which *k(x,y)* are the values of the argument of the Bessel functions corresponding to their extrema. Zero-order dark fringes appear when the intensity value, given by equation (13), is zero. This condition corresponds to $k=0$, because $J_0(0)=1$ then $1-J_0(0)=0$ and, from equation (16), the vibration amplitude is also zero, representing nodal regions. The fringe contrast decrease quickly starting from the zero order on. As the present study and the experiment were not designed to obtain the full field vibration amplitude, only a particular direction along the object was chosen to perform vibration amplitude measurements. Let us take as an example the interferogram corresponding to a resonant frequency of 2.7 kHz for the plate having a concentrated mass, as it is shown in Fig. 6(a), where a particular direction AB, is indicated. To remove some of the speckle noise and to make the speckle interferogram smoother, several interferograms corresponding to the same normal mode (taken at different times) were added, resulting in the interferogram of Fig. 6(a). To reduce noise even further, the profile shown in Fig. 6(b) is obtained by averaging pixel values of several rows adjacent to the line AB.

Along this direction, the corresponding fringe profile, shown in Fig. 6(b) was analyzed to locate the coordinates of the centre of bright and dark fringes, the extrema of the Bessel function, and to associate the corresponding argument, *k(x,y)*. By means of equation (16), the corresponding amplitude of vibration was calculated. The results are shown in Fig. 7, together with the curve calculated by means of the analytical methods using equation (7).

As the excitation energy is unknown, it is not possible to calculate the vibration amplitude. So, the analytical curve has been multiplied by a constant factor in order to compare

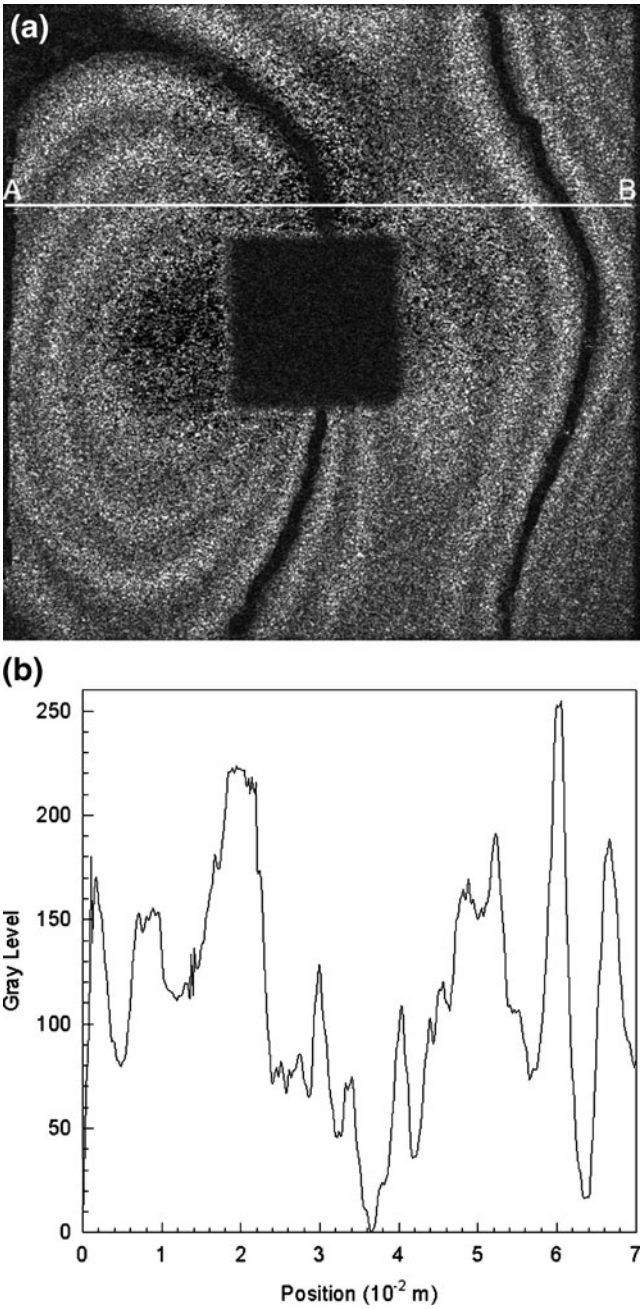

Fig. 6 (**a**) Fringe pattern corresponding to the plate with concentrated mass vibrating at 2.7 kHz (**b**) Fringe profile along the direction indicated in (**a**)

it with the experimental results. This constant was obtained by means of an iteration process in which the mean deviation between the experimental and analytical sets of data is minimized. A mean deviation of 0.004 λ was found representing approximately 0.6% of the maximum deflection of the plate.

Conclusions and Discussions

We have presented a study of vibrating plates, in which analytical solution and experimental measurements are compared. DSPI was successfully used to determine resonant frequencies and modal shapes of perforated plates subjected to a certain boundary condition. This real-time determination of resonant frequencies and mode shapes of vibrating plates has large number of applications in industry for nondestructive evaluation of the components. The experimental device is very simple to implement and exhibits great sensitivity for tuning resonant frequencies. Values of resonant frequencies, obtained by both analytical and experimental methods, are closely correlated taking into account the estimated errors in the measurements of the involved parameters. Qualitatively, the mode shapes as well as the nodal patterns match remarkably with the predictions of the computational method. As it is stated in "Amplitude Measurements", the contrast of the correlation fringes decreases quickly from the zero order on; thus, limiting the number of good visibility of fringes. However, amplitude measurements have also been carried out experimentally for a particular case and they show a reasonable agreement with the analytical results. Further studies including full field deformation measurements in this type of mechanical system and in anisotropic material are in progress.

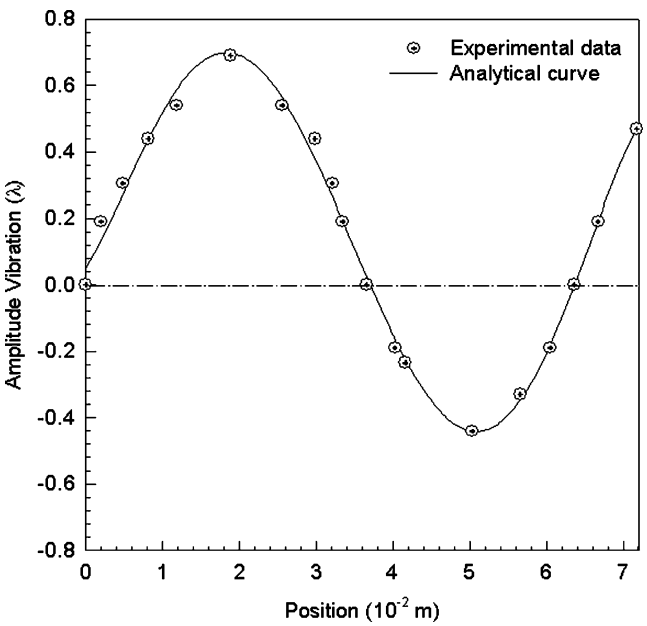

Fig. 7 Amplitude of vibration along the line AB of Fig. 6(**a**), determined experimentally (*dots*) and analitically (*continuous line*)

Acknowledgements This work was supported by ANPCyT Contrato de Préstamo BID 1728/OC-AR and Consejo de Investigación Project Nº 1571 of the Universidad Nacional de Salta.

References

1. Lekhtnitskii SG (1968) Anisotropic plates. Gordon and Breach Science, New York
2. Panteghini A, Genna F, Piana E (2007) Analysis of a perforated panel for the correction of low frequency resonances in medium size rooms. Appl Acoust 68(10):1086–1103
3. Felix DH, Bambill DV, Rossit CA, Rossi RE, Laura PA (2003) Natural frequencies of a vibrating repaired panel in an ocean structure. Ocean Eng 30:955–963
4. Weaver W Jr, Timoshenko SP, Young DH (1990) Vibration problems in engineering. Wiley, New York
5. Romero G, Alvarez L, Alanís E, Nallim L, Grossi R (2003) Study of a vibrating plate: comparison between experimental (ESPI) and analytical results. Opt Lasers Eng 40:81–90
6. Nallim LG, Grossi RO (2001) Natural frequencies of edge restrained tapered, isotropic and orthotropic rectangular plates with a central free hole. Appl Acoust J 61:289–305
7. Bhat RB (1985) Natural frequencies of rectangular plates using characteristic orthogonal polynomials in Rayleigh–Ritz method. J Sound Vib 102:493–499
8. Harabovsky M, Smid O, Horváth P, Baca Z (2002) Measurement of object vibrations using the theory of speckle pattern decorrelation. Optik 113(3):117–120
9. Kauffmann J, Tiziani H (2006) Time-resolved vibration measurement with temporal speckle pattern interferometry. Appl Optics 45 (26):6682–6688
10. Jin F, Chiang FP (1998) ESPI and digital speckle correlation applied to inspection of crevise corrosion on ageing aircraft. Res Nondestr Eval 10(2):63–73
11. Demoli N, Vukisevic D (2004) Detection of hidden stationary deformations of vibrating surfaces by use of time-average digital holographic interferometry. Opt Lett 29(20):2423–2425
12. Asundi A, Raj Singh V (2006) Time-averaged in-line digital holographic interferometry for vibrations analysis. Appl Optics 45 (11):2391–2395
13. Keene L, Chiang F-Pen (2009) Real-time anti-node visualization of vibrating distributed systems in noisy environments using defocused laser speckle contrast analysis. J Sound Vib 320:472–481
14. Ennos E (1984) Speckle interferometry. In: Dainty JC (ed) Laser speckle and related phenomena, vol 9. Springer, Berlin
15. Vest CM (1979) In: Ballard SS (ed) Holographic interferometry. Wiley, New York
16. Coggrave CR, Huntley JM (2004) Real-time visualization of deformation fields using speckle interferometry and temporal phase unwrapping. Opt Lasers Eng 41(4):601–620
17. Aguanno M, Lakestani F, Whelan P, Connelly M (2007) Heterodyne speckle interferometer for full-field velocity profile measurements of a vibrating membrane by electronic scanning. Opt Lasers Eng 45(6):677–683
18. Kumar R, Shakher C (2004) Applications of digital speckle pattern interferometry and wavelet transform in measurement of transverse vibrations in square plate. Opt Lasers Eng 42(5):585–602
19. Borza D (2008) Speckle noise reduction in vibration measurements by time-average speckle interferometry and digital holography a unifying approach. J Solid Mech Mater Eng 2 (6):695–706
20. Warburton GB, Edney S (1984) Vibrations of rectangular plates with elastically restrained edges. J Sound Vib 95:537–552
21. Mukhopadhyay M (1987) Vibration analysis of elastically restrained rectangular plates with concentrated masses. J Sound Vib 113:547–558
22. Bhat RB (1985) Plate deflection using orthogonal polynomials. J Eng Mech 101:1301–1309